1994PASJ...46L.151H

LETTER

PASJ: Publ. Astron. Soc. Japan **46**, L151–L155 and Plate 8–10 (1994)

ASCA Observations of Cassiopeia A

Stephen S. HOLT and Eric V. GOTTHELF
NASA/Goddard Space Flight Center, Greenbelt, MD 20771, USA
and
Hiroshi TSUNEMI and Hitoshi NEGORO
Earth and Space Science, Faculty of Science, Osaka University, 1-1 Machikaneyama-cho, Toyonaka, Osaka 560

(Received 1994 March 11; accepted 1994 May 25)

Abstract

The ASCA Observatory provides the first capability to map a diffuse X-ray source in individually resolved emission lines. We have applied this capability to the Cas A supernova remnant, measuring the mean energies and equivalent widths of 14 line features in three distinct spatial regions. The northwest (NW) and southeast (SE) regions provide the large fraction of the X-ray emission at energies below 4 keV, and define the axis of a Doppler map of the remnant constructed by measuring the peak energy of the prominent Si-K feature. Using restoration techniques to obtain image quality equivalent to 30″ FWHM, we present restored images in the two brightest line features, and in two continuum bands. An emission region in the west is increasingly prominent at higher energies, and its markedly lower metallicity and correlation with radio emission suggest that its X-ray emission has a larger component from fore-shocked material than do the NW and SE regions where the emission is presumed to be dominated by reverse-shocked material.

Key words: ISM: individual objects: Cas A — ISM: supernova remnants — X-rays : interstellar

1. Introduction

Cas A is the youngest known supernova remnant in our galaxy, with an age of $\sim$ 300 yr. Unlike the slightly older remnants observed by (and named for) Kepler and Tycho, both of which are usually classified as Type I, Cas A is considered to have evolved from a massive progenitor on the basis of heavy element enrichment observed in optical and X-ray emission lines (see Raymond 1984 and references therein). The optical lines are associated with both fast moving (up to 6000 km s^{-1}) oxygen-rich knots presumed to be undiluted supernova ejecta and more slowly moving ($<$ 200 km s^{-1}) material thought to be pre-supernova outflow from the progenitor star. Cas A is a relatively strong X-ray source, with most of its emission in the few keV band arising from a clumpy "shell" of reverse-shocked ejecta with average radius 102″ and thickness 17″ (Fabian et al. 1980). An outer "shell" of radius 150″ arises from the interaction of the primary shock with the ISM, but the reverse-shocked ejecta dominates because of its higher density, lower temperature, and higher metallicity.

Cas A was one of the first sources from which X-ray Fe-K emission lines were unambiguously observed with proportional counters (Serlemitsos et al. 1973). The factor-of-six increase in energy resolving power of the Solid State Spectrometer (SSS) on board the Einstein Observatory provided for the detection of K-emission lines from Mg, Si, S, and Ar; the spectrum was fit with a simple whole remnant two-temperature coronal equilibrium model in order to make a first attempt at X-ray determined elemental abundances (Becker et al. 1979). Observations of Cas A with the gas scintillation proportional counters on board the Tenma and EXOSAT Observatories allowed the simultaneous observation of the Si-K and S-K lines with the Fe-K lines and the high energy continuum. Despite the poorer spectral resolution of these detectors (relative to the SSS), their extended energy range demonstrated the inadequacy of the two-temperature thermal equilibrium model (Jansen et al. 1988). Analyses of these data suggested that non-equilibrium ionization, which could be applied with some success to young Type I remnants with relatively homogeneous shell structure, might also be invoked to reconcile the more heterogeneous morphology of Cas A (Tsunemi et al. 1986).

This paper describes observations of Cas A made with the ASCA Observatory (Tanaka et al., 1993) during its Performance Verification (PV) phase. ASCA combines broad-band imaging capability with spectral resolution better than that of the SSS.

2. Observations

The ASCA Observatory consists of four co-aligned telescopes, each of which couples a conical foil mirror to one of two types of imaging spectrometers. The data

© Astronomical Society of Japan • Provided by the NASA Astrophysics Data System

1994PASJ...46L.151H

Table 1. X-ray line features identified in Cas A (all energies in keV.)

Line Name	Lab Energy	Southeast Energy(error)	Southeast EW (keV)	Northwest Energy(error)	Northwest EW (keV)	West Energy(error)	West EW (keV)
Ne Lyα	1.02	1.0177(0.0020)	0.08	1.0207(0.0016)	0.07	1.0198(0.0027)	0.06
Fe-L	1.08	1.0889(0.0032)	0.05	1.0960(0.0051)	0.02	1.0929(0.0071)	0.02
Mg Heα	1.35	1.3535(0.0019)	0.05	1.3513(0.0017)	0.05	1.3503(0.0024)	0.04
Mg Lyα	1.48	1.4883(0.0031)	0.05	1.4788(0.0034)	0.02	1.4824(0.0040)	0.03
Si Heα	1.85	1.8601(0.0003)	0.63	1.8504(0.0003)	0.57	1.8524(0.0005)	0.41
Si Lyα	2.00	2.0063(0.0013)	0.13	1.9970(0.0015)	0.11	1.9968(0.0005)	0.10
Si Heβ	2.20	2.2002(0.0015)	0.14	2.1967(0.0017)	0.13	2.1996(0.0025)	0.11
Si Lyβ	2.40	2.3943(0.0158)	0.19	2.3099(0.0660)	0.03	2.3075(0.1027)	0.03
S Heα	2.45	2.4573(0.0009)	0.43	2.4360(0.0007)	0.52	2.4398(0.0011)	0.39
S Lyα	2.62	2.6319(0.0052)	0.05	2.6178(0.0050)	0.04	2.6172(0.0059)	0.06
S Heβ	2.89	2.8936(0.0049)	0.05	2.8919(0.0058)	0.06	2.8832(0.0068)	0.05
Ar Heα	3.12	3.1291(0.0024)	0.19	3.1146(0.0025)	0.17	3.1155(0.0035)	0.15
Ca Heα	3.87	3.8805(0.0052)	0.11	3.8653(0.0048)	0.10	3.8630(0.0070)	0.08
Fe Heα	6.60	6.6080(0.0049)	1.26	6.5568(0.0043)	1.03	6.5916(0.0064)	0.65

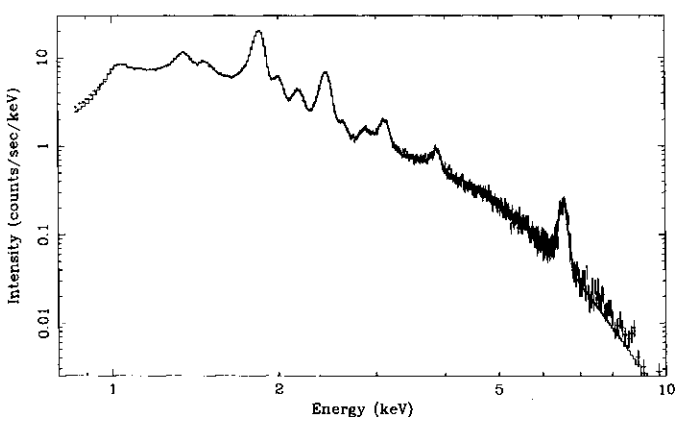

Fig. 2. The ASCA SIS 0 pulse-height spectrum of the bright NW knot of Cassiopeia A.

presented here are from the Solid State Imaging Spectrometers (SIS; Inoue 1993), with intrinsic spatial resolution sufficient to oversample the telescope Point Spread Function (PSF) and spectral resolution of approximately 100 eV FWHM over the energy band 0.4–10 keV. The PSF exhibits a sharp core with on-axis FWHM of 50″, but with extended wings resulting in a total half power diameter of 3′ (see Jalota et al. 1993; Serlemitsos et al. 1994).

Two consecutive observations of Cas A, offset by $\sim$ 6′ from each other, were carried out on 1993 August 1 for effective times of 15 ks and 12 ks. The spatial extent of Cas A is well matched to a single SIS CCD, and all data were collected in "one CCD mode"; this placed the images of Cas A between 3′–12′ off-axis. Figure 1 (Plate 8) displays the broad-band image obtained with SIS 0 during the second pointing, which has been aspected, time filtered, and cleaned of CCD anomalies, along with the result of image restoration using the algorithm of Lucy (1974) and Richardson (1972). In addition to emphasizing the dominant diffuse areas in the NW and the SE, the restoration also reveals a more concentrated area in the northeast and a weaker diffuse area in the west. It is reassuring that the structure in the image mimics that which is seen with the Einstein High Resolution Imager (HRI) (Murray et al. 1979). The broad-band ASCA CCD images are similar to the HRI image smeared out to an apparent resolution of $\sigma \sim 12''$ (gaussian), comparable to the core of the ASCA PSF. A complete description of the techniques used to restore the Cas A images presented here, and the application of image restoration techniques to ASCA data in general, can be found in Gotthelf (1994).

3. Analysis

The data discussed here are all those from both exposures of SIS 0, so that while the effective energy resolution is poorer than it could be if the data sample was further restricted, all portions of the remnant are uniformly compromised. Figure 2 displays the pulse-height spectrum extracted from the bright NW region of Cas A. It cannot be well-fitted with a single-T coronal equilibrium spectrum, so that we present a heuristic fit with an absorbed power law continuum and 14 gaussians. The latter are summarized in table 1, and are associated with features expected in emission spectra of hot plasmas. Lyα and Lyβ are the analogs of Lyman α and Lyman β in

© Astronomical Society of Japan • Provided by the NASA Astrophysics Data System

1994PASJ...46L.151H

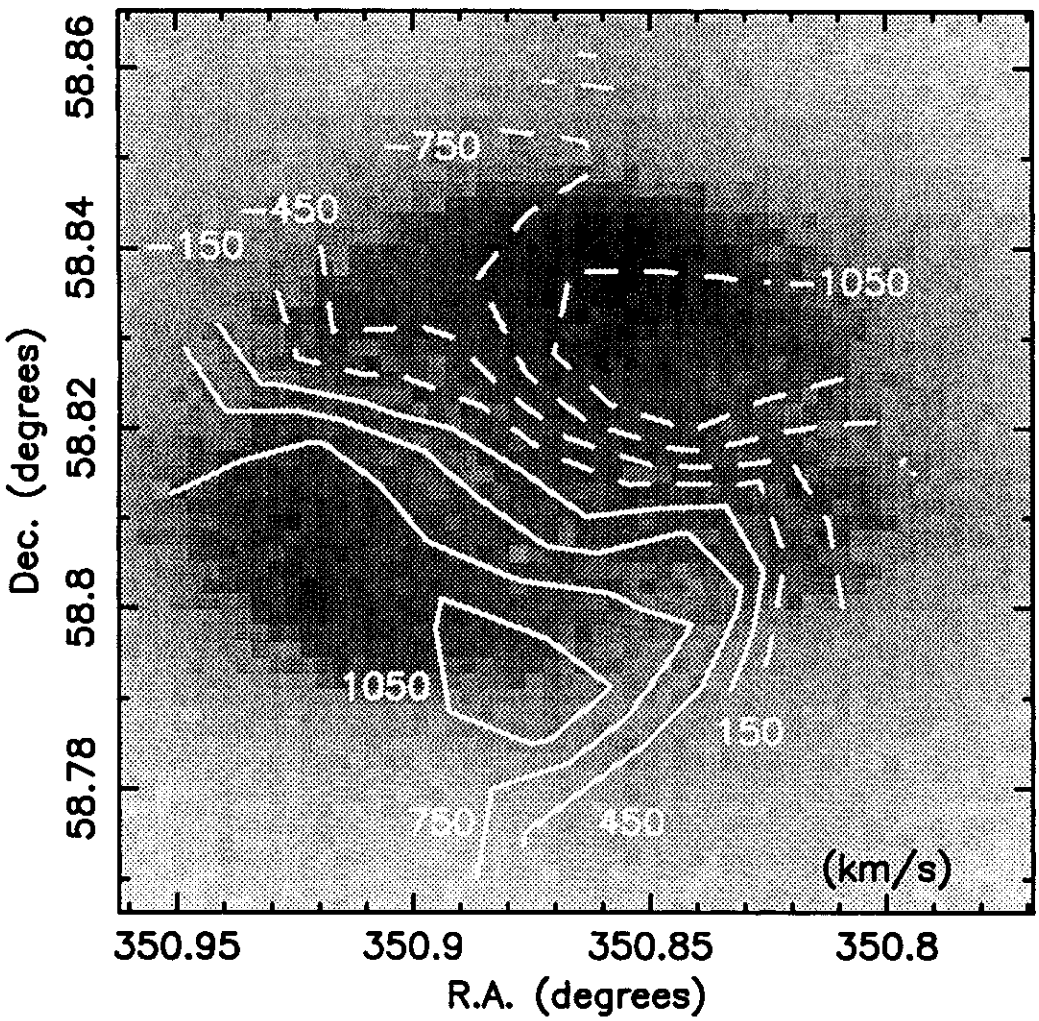

Fig. 3. Doppler contour map (equinox J2000) of the peak energy of the 1.85 keV Si line of Cassiopeia A.

hydrogen-like ions; Heα and Heβ are the same for helium-like ions. The He-like "lab" energies given in table 1 are for the resonance lines, but Cas A equivalents will include other components of the He-like blends and will also be broadened on the red side by contamination from lower ionization states. The entry marked Fe L is meant to be a broad combination of L lines from a variety of ionization states of Fe. The measured values of peak energies and equivalent continuum widths (EW) are given in the appropriate columns of the table with the one-σ statistical errors to the line fit in parentheses. It is important to note that the response functions used for this analysis are still preliminary at the time of this writing, so that while the relative energy separations can be assumed to be correct at the 1 eV level, the absolute energy calibration can be off by $\sim$ 10 eV.

It is clear from table 1 that the systematic Doppler variation from the NW to the SE described by Markert et al. (1983) is easily observable here. It is also clear that the average velocities seen in the west are closer to those in the NW than in the SE. Virtually none of this apparent Doppler morphology can be attributable to the CTI (charge transfer inefficiency) of the CCDs. Although the far end of the image is transferred through some 200 more pixels than is the near end, our observations of Cas A at two different positions on the chip allow a direct measurement of the CTI of 5×10^{-6}, or an apparent energy difference of no more than a few eV across the remnant. A "Doppler map" of Cas A is exhibited in figure 3, constructed from $1' \times 1'$ sliding box samples (50% overlap) of the peak energy of the 1.85 keV feature. It is conceivable that there is some non-Doppler contamination of this map from differences in the Si ionization structure across the remnant; this could be avoided by using the completely resolved 2 keV Si Lyα line, but its poorer statistics do not allow this spatial resolution. The fact

© Astronomical Society of Japan • Provided by the NASA Astrophysics Data System

1994PASJ...46L.151H

that the plasma conditions appear to be similar across the remnant (i.e., there are no clear systematic differences in the relative strengths of the multiple lines of either Si or S with position) suggests that the map therefore displays true Doppler variation across the remnant of > 2000 km s^{-1}.

Figure 4 (Plate 9) exhibits narrow band line images of Si Heα and S Heα, with and without image restoration. It should not be surprising that the Si Heα image is similar to that for the broad-band spectrum, as this line complex is the major contributor to the detected source photons (all the lines exhibit similar morphology, i.e., arising primarily in the same two extended emission regions). Figure 5 (Plate 10) exhibits a similar pair of images from two "continuum" spectral regions which are relatively free of line contamination: energies between the resolved Mg and Si K lines, and between the resolved Ca and Fe K lines. In marked contrast to the line emission, the relative continuum contribution in the west is much stronger and harder, with $\alpha = 1.74 \pm .01$ vs. $2.04 \pm .01$ (SE) and $1.90 \pm .01$ (NW).

4. Discussion

Early fits to X-ray data from SNRs were done with coronal equilibrium spectra, wherein the ionization state of each species is determined entirely from collisions, and the electron and ionization temperatures of the plasma are the same. More realistic calculations of the X-ray spectra associated with SNRs were calculated by Itoh (1977), based on the realization that the material shocked to X-ray temperatures in young adiabatic remnants does not have time to equilibrate with the shock, and will be under-ionized. A variety of such NEI (non-equilibrium ionization) calculations were performed in order to explain the Einstein, EXOSAT, and Tenma observations. For example, the general framework developed by Hamilton et al. (1983) to handle the Sedov (fore-shock) components of adiabatic remnants could be applied (although with parameters that might be artificial) to the X-ray emission from non-homogeneous material and the reverse-shocked ejecta (see Hamilton 1985 and references therein).

If we can find NEI models that give reasonable values of nt (the product of the electron density with the time since the shock began to ionize the material) we might be able to translate the results into abundances, but NEI calculations for the three areas are not consistent with either the same nt for all elements or with an "onion-skin" having clear monotonic Z-dependence. Previous reports of optical measurements of individual knots which appear to be mono-elemental make it clear that simple NEI models for Cas A will never be sufficient for its detailed description. It should also be noted that small changes in the final response function can substantially change the results of NEI calculations, since most of the statistical significance in each spectrum is determined by the "He-like" complexes which are combinations of all the lower ionization states. Awaiting a more careful attempt at these calculations when the final response functions are available, typical values obtained here from the NEI calculations for Si are $nt = 10^{11}$ s cm^{-3} and $kT = 1.8$ keV, and for S are 2×10^{11} s cm^{-3} and 1.4 keV.

The conventional wisdom is that the X-ray emission from Cas A is dominated by the reverse-shocked ejecta, with a more tenuous hot fore-shocked shell at radii $> 102''$ (Fabian et al. 1980; Jansen et al. 1988). A qualitative description of the ASCA data is that the NW and SE emission regions are, indeed, such ejecta-rich reverse-shocked volumes, moving outward from the remnant center in accordance with their relative average Doppler motion. The surprising new result from the ASCA images, demonstrated most dramatically from the model-independent image restoration, is that at increasingly higher energies the western region becomes more prominent, especially in the continuum (previous measurements with Einstein and ROSAT showed spectral hardening in the west, but only at energies < 4 keV). This is quantitatively borne out by table 1, wherein it is clear that the equivalent widths of the lines are systematically lower in the west than in the other two large emission regions. And, since the extended wings of the mirror PSF are comparable with the size of the remnant, the values of EWs that are highest must be considered lower limits, and the lowest EWs (in particular, those in the west) must be considered upper limits.

A simple explanation for this morphology is that the west contains a high column density of ISM fuel for the fore-shock, and therefore exhibits high surface brightness with lower metallicity than the reverse-shocked ejecta. The hot continuum is a measure of electrons at X-ray temperatures; simple first-order shock theory can explain why the temperature should be higher in the fore-shocked than in the reverse-shocked material (Jansen et al. 1988), but cannot explain the presence of relativistic electrons (see Anderson et al. 1991 for a discussion of the failure of simple shock models to describe the spatial and spectral radio measurements of Cas A). Nevertheless, the radio maps of Cas A in Anderson et al. (1991) are morphologically similar to those in X-rays, especially those of the "continua" displayed in figure 5 (Plate 10): each have two bright areas in the NW and SE on a ring with diameter consistent with the reverse-shock, a smaller feature in the northeast on the same ring, and a bright enhancement in the west on an angular scale extending beyond the ring.

© Astronomical Society of Japan • Provided by the NASA Astrophysics Data System

1994PASJ...46L.151H

References

Anderson M., Rudnick L., Leppik P., Perley R., Braun R. 1991, ApJ 373, 146

Becker R.H., Holt S.S., Smith B.W., White N.E., Boldt E.A., Mushotzky R.F., Serlemitsos P.J. 1979, ApJL 234, L73

Fabian A.C., Willingale R., Pye J.P., Murray S.S., Fabbiano G. 1980, MNRAS 193, 175

Gotthelf E.V. 1994, Experimental Astron. in press

Hamilton A.J.S. 1985, ApJ 291, 523

Hamilton A.J.S., Sarazin C.L., Chevalier R.A. 1983, ApJS 51, 115

Inoue H. 1993, Experimental. Astron. 4, 1

Itoh H. 1977, PASJ 29, 813

Jalota L., Gotthelf E.V.,Zoonermatkermani S. 1993, Proc. SPIE 1945, 453

Jansen F., Smith A., Bleeker J.A.M., de Korte P.A.J., Peacock A., White N.E. 1988, ApJ 331, 949

Lucy L. 1974, AJ 79, 745

Markert T.H., Canizares C.R., Clark G.W., Winkler P.F. 1983, ApJ 268, 134

Murray S.S., Fabbiano G., Fabian A.C., Epstein A., Giacconi R. 1979, ApJL 234, L69

Raymond J.C. 1984, ARA&A 22, 75

Richardson W.H. 1972, J. Opt. Soc. Am. 62, 55

Serlemitsos P.J., Boldt E.A., Holt S.S., Ramaty R., Brisken A.F. 1973, ApJL 184, L1

Serlemitsos P.J. et al. 1994, PASJ in press

Tanaka Y., Inoue H., Holt S.S. 1994, PASJ 46, L37

Tsunemi H., Yamashita K., Masai K., Hayakawa S., Koyama K. 1986, ApJ 306, 248

© Astronomical Society of Japan • Provided by the NASA Astrophysics Data System

1994PASJ...46L.151H

© Astronomical Society of Japan • Provided by the NASA Astrophysics Data System